# Investigation on the Correlations between Droplet and Particle Size Distribution in Ultrasonic Spray Pyrolysis

**ARTICLE** *in* INDUSTRIAL & ENGINEERING CHEMISTRY RESEARCH · JANUARY 2008

Impact Factor: 2.59 · DOI: 10.1021/ie070821d



**6 AUTHORS**, INCLUDING:

Wei-Ning Wang
Virginia Commonwealth University
**92** PUBLICATIONS **1,826** CITATIONS
SEE PROFILE

Agus Purwanto
Universitas Sebelas Maret
**60** PUBLICATIONS **471** CITATIONS
SEE PROFILE

Wuled Lenggoro
Tokyo University of Agriculture and Technology
**122** PUBLICATIONS **3,229** CITATIONS
SEE PROFILE

Hee Dong Jang
Korea Institute of Geoscience and Mineral Re…
**140** PUBLICATIONS **1,921** CITATIONS
SEE PROFILE

GENERAL RESEARCH

# Investigation on the Correlations between Droplet and Particle Size Distribution in Ultrasonic Spray Pyrolysis

**Wei-Ning Wang,[†] Agus Purwanto,[†] I. Wuled Lenggoro,[‡] Kikuo Okuyama,*[,†] Hankwon Chang,[§] and Hee Dong Jang[§]**

*Department of Chemical Engineering, Graduate School of Engineering, Hiroshima University, Higashi Hiroshima, 739-8527, Japan, Institute of Symbiotic Science and Technology, Tokyo University of Agriculture and Technology, Koganei, Tokyo, 184-8588, Japan, and Minerals & Materials Processing Division, Korea Institute of Geoscience & Mineral Resources (KIGAM), Daejeon 305-350, Korea*

In this study, the measurement of droplet size distribution by means of a laser diffraction technique in ultrasonic spray pyrolysis was investigated. Effects of precursor temperature, spray volume rate, carrier gas flow rate, and physicochemical properties of precursors were analyzed in detail. The results showed that the mean size of precursor droplets decreased with increasing precursor temperature, concentration, and addition of alcohol, while it increased with increasing spray volume rate and carrier gas flow rate. Bimodal droplet size distribution was observed probably due to droplet coagulation effect. A cyclone or an impactor was used to control the droplet size distribution. Uniform droplets were obtained using a cyclone that removed large droplets. For comparison, spray pyrolysis of salt aqueous solutions, such as $ZrO(NO_3)_2$ and $Ni(NO_3)_2$, were also conducted. Particle size distribution of the spray pyrolyzed powders was analyzed using scanning electron microscopy. The results showed that the particle size distribution of prepared solid particles was strongly dependent on, and could be controlled by, variation in the corresponding properties of the sprayed droplets.

## 1. Introduction

The synthesis of fine particles (i.e., from submicrometer to micrometer) with controlled particle size (PS) and particle size distribution (PSD) has attracted increasing attention in recent years. An unagglomerated spherical particle with a narrow size distribution is preferred for many applications, especially for the compacting and sintering of particles.[1] Traditionally, mechanical milling was used for particle micronization. However, intensive milling can create amorphous regions or defects on particle surfaces, which can affect humidity dependence and stability, electrostatic charging, and cohesivity.[2] Recently, wet chemical techniques such as sol−gel and hydrothermal methods have been widely studied. However, mean particle size and particle size distribution of the resulting particles are sometimes not controlled. In addition, long reaction and posttreatment times are usually required, and impurities may be introduced during the various steps of preparation.

It is important to develop a process in which particle characteristics including mean size, size distribution, morphology, and composition can be controlled easily. To be industrially relevant, the process needs to be low cost and capable of both continuous operation and high production rates. One of the candidate methods used to fulfill these requirements is spray pyrolysis. It has a number of inherent advantages: the particles produced are spherical, uniform in size and composition; multicomponent (composite) materials are easily produced; the process is continuous, simple, and low cost.[1]

To prepare particles by spray pyrolysis, a precursor solution is prepared by dissolving, usually, the metal salts of the product in the solvent. The droplets are atomized from the precursor solution by an atomizer (e.g., ultrasonic nebulizer), and are then introduced to a reactor. Evaporation of solvent, precipitation of solutes, drying, reaction/pyrolysis, or sintering may occur inside the droplets to form the final product.[3] Generally, one-droplet-to-one-particle (ODOP) conversion is considered to be the typical particle formation mechanism in conventional spray pyrolysis (CSP), based on the mass conservation law.[1,3,4] Following the ODOP principle, it is obvious that the droplet characteristics, e.g., droplet mean size and size distribution, have a direct relationship with those of the product particles. It is essential to investigate various factors related to the droplet size measurement.

In spray pyrolysis processes, a two-fluid nozzle and an ultrasonic nebulizer are generally used as atomizers, and the ultrasonic nebulizer has the advantage of generating droplets with a narrower size distribution than those from the two-fluid nozzle. In addition, ultrasonic technology has recently improved intensively and received increasing attention for applications in atomization, analytical chemistry, industry cleaning, separation, and so on.[5−8] For these reasons, the ultrasonic nebulizer was selected in this work for investigation. Size measurement of droplets generated by an ultrasonic nebulizer has been investigated by many researchers using different techniques, such as laser diffraction and image processing.[9−15] Typically, the mean droplet size produced by an ultrasonic nebulizer is expressed by Lang's equation:

* To whom correspondence should be addressed.: Tel.: +81-82-424-7716. Fax: +81-82-424-5494. E-mail: okuyama@hiroshima-u.ac.jp.

[†] Hiroshima University.

[‡] Tokyo University of Agriculture and Technology.

[§] KIGAM.

10.1021/ie070821d CCC: $40.75 
Published on Web 01/23/2008

$$d_d = 0.34\left(\frac{8\pi\gamma}{\rho f^2}\right)^{1/3} \quad (1)$$

However, no dependence of viscosity on the mean droplet size was provided, which is contrary to the experimental observations. Rajian et al.[16] proposed an empirical correlation considering the dependence on almost all physicochemical properties of the liquid atomized as follows:

$$d_d = \text{constant}(f)^{-0.66}(Q)^{0.207}(\gamma)^{0.11}(\rho)^{-0.274}(\eta)^{0.166}(\text{power/area})^{-0.4} \quad (2)$$

Generally, from eq 2, we can conclude that the size of droplets generated from an ultrasonic nebulizer is directly proportional to the liquid flow rate, surface tension, and viscosity of precursors, and is inversely proportional to frequency and precursor density. However, other important factors, such as carrier gas flow rate and droplet number concentration in an arbitrary volume (e.g., in a tubular reactor), have rarely been investigated. In addition, to obtain uniform particles, control of droplet size distribution is necessary to be carried out. A cyclone and a T-type impactor were selected for this purpose in this study.

Many researchers have reported on the preparation of fine and ultrafine particles using the spray route.[4,6,17,18] However, little research focusing on the correlations between the mean size and size distribution of droplets and prepared particles in spray pyrolysis process has been reported.[2,4] Elversson et al. reported on the droplet and particle size relationship in a spray-drying process.[2] A two-fluid nozzle was used as the atomizer. The effects of nozzle orifice diameter, atomization air flow, and feeding concentration on droplet and particle size were examined. However, the resultant particles were hollow in morphology with a broad size distribution, which was difficult to evaluate directly based on the mass conservation law. The droplet-to-particle conversion in spray pyrolysis is considered more complicated than that in the spray-drying process, due to many physical and chemical phenomena such as nucleation, crystalline growth, thermal reaction, and gas evolution.

The objectives of this work were (1) to measure the size distribution of droplets generated by an ultrasonic nebulizer. Effects of precursor temperature, carrier gas flow rate, spray volume rate, solution concentration, and precursor physical properties were investigated systematically. Necessary conditions for generation of droplets with unimodal as well as bimodal size distribution from precursor solutions in the ultrasonic nebulizer were observed and suggested. (2) Next, control of droplet size distribution was conducted by means of a cyclone and a T-type impactor. (3) For comparison, spray pyrolysis of salt aqueous solutions ($ZrO(NO_3)_2$ and $Ni(NO_3)_2$) was also conducted. The role of droplet size distribution in the control of spray pyrolyzed particle size characteristics in the CSP process were investigated. The correlations between droplet and particle sizes were discussed based on the ODOP principle.

## 2. Experimental Section

**2.1. Ultrasonic Nebulizer System.** An ultrasonic nebulizer (NE-U17, Omron Healthcare Co. Ltd., Tokyo, Japan) operated at 1.7 MHz was used for droplet generation. It is capable of a spray volume rate of as much as $2.78 \times 10^{-8}$ $m^3/s$, depending on the physicochemical properties of precursors, power applied, carrier gas flow rate, and so on. When pure water was used as the precursor, the water temperature was altered at 288, 293, 298, 303, 308, and 313 K. For other precursors, the precursor temperature was maintained constant at 293 K. To keep the liquid surface at the same level, the precursor was supplied and cycled using a peristaltic pump (PST-350, Iwaki Asahi Techno Glass Co., Tokyo, Japan). A homemade cyclone and a T-type impactor were used for cutting the very large droplets (e.g., above 10 $\mu$m) to obtain a relatively sharp droplet size distribution. In the case of the cyclone system, a T-type impactor was always in series with the cyclone.

**2.2. Laser Diffraction Technique.** A spray particle analyzer system (Spraytec, Malvern Instruments Ltd., Malvern, U.K.) was used for droplet size measurement. This is a diode laser based system, with a wavelength of 670 nm and a beam diameter of $1.0 \times 10^{-2}$ m. It is designed to continuously measure particle size distribution information and is able to measure particles at measurement rates up to 2.5 kHz. The schematic diagram of the experimental setup is shown in Figure 1a. The resolution of the droplet size is dependent on the lens size and the laser beam diameter. For this study, a 100 mm lens was used, and the measurable droplet size ranged from $1.0 \times 10^{-7}$ m (0.1 $\mu$m) to $2.3 \times 10^{-4}$ m (230 $\mu$m). For convenience, micrometers will be used as the unit of droplet/particle size throughout the following sections. The working distance between the spray particles and the lens system ($L_1$) and distance between the nozzle exit/mouth and the laser beam ($L_2$) were fixed at $7.0 \times 10^{-2}$ and $3.0 \times 10^{-2}$ m, respectively. All measurements were performed in a dark room to eliminate the influence of natural/outside lights and in ambient temperatures of 290−300 K with relative humidity of 40−70%, which are conditions similar to those of the spray pyrolysis experiments. The shape of droplet size distribution was described by the span value, which was defined as follows:[2,11]

$$\text{span} = \frac{d_{v,90} - d_{v,10}}{d_{v,50}} \quad (3)$$

The sharpness of the droplet size distribution increases with decreasing span value. $d_{v,50}$ will be used as the mean diameter of droplets. The size of droplets, or particles, refers to the diameter in this paper, unless otherwise stated.

**2.3. Physical Property Measurement of Precursors.** The physicochemical properties of a liquid, e.g., refractive index, surface tension, viscosity, and density, may have a strong influence on the formation of droplets and their size characteristics. The refractive indices of solutions, $n$, were calculated using the Maxwell Garnett mixing rule (Table 1).[19,20] From the table, we find that, for aqueous solutions with low density and concentration, refractive indices do not differ significantly from that of pure water. Viscosity, surface tension, and density were characterized using a programmable rheometer (DV-III Ultra, Brookfield Engineering Labs, Middleboro, MA), a surface tensiometer (CBVP-Z, Kyowa Interface Science Co., Ltd., Saitama, Japan), and an electronic analytical balance in conjunction with a density determination kit (AG-204, Mettler-Toledo GmbH, Laboratory & Weighting Technologies, Switzerland), respectively. The physical data, both cited and measured, of precursors tested are listed in Table 1.

**2.4. Spray Pyrolysis Procedure.** A schematic diagram of the spray pyrolysis experimental setup can be found in Figure 1b, and the detailed explanation of the experimental procedures was given in our previous publications.[4,17,21] The process consists of an ultrasonic nebulizer, a ceramic tubular reactor with an inner diameter of $1.3 \times 10^{-2}$ m, a length of 1.0 m, and a glass filter for collecting particles. Nickel nitrate hexahydrate ($Ni(NO_3)_2 \cdot 6H_2O$) and zirconyl nitrate dihydrate ($ZrO(NO_3)_2 \cdot$

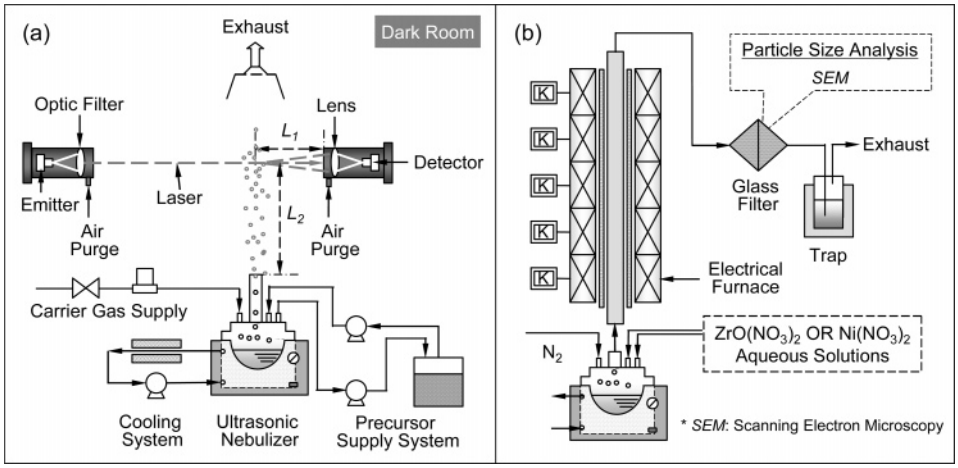


**Figure 1.** (a) Schematic diagram of droplet size measurement by means of the Spraytec and (b) experimental setup of spray pyrolysis using an ultrasonic nebulizer as the atomizer.

**Table 1. Physical Properties of Precursors Used in the Experiment (at 293 K,[a] 1.01 × $10^5$ Pa)**

| precursors | $T$ [K] or $C$ [mol/m$^3$] | $\rho \times 10^{-3}$ [kg/m$^3$] | $\eta/10^{-3}$ [Ns/m$^2$] | $\gamma$ [N/m] | $n^b$ | $P$ [kPa] | memo |
|---|---|---|---|---|---|---|---|
| $H_2O$ | 288 | 0.9991 | 1.140 | 73.5 | 1.3335 | 1.706 | data from CRC Handbook[31] |
| | 293 | 0.9982 | 1.002 | 72.75 | 1.3318c | 2.339 | |
| | 298 | 0.9970 | 0.894 | 72.00 | 1.3325 | 3.169 | |
| | 303 | 0.9957 | 0.797 | 71.20 | 1.3320 | 4.246 | |
| | 308 | 0.9940 | 0.723 | 70.40 | 1.3312 | 5.627 | |
| | 313 | 0.9922 | 0.653 | 69.60 | 1.3305 | 7.381 | |
| EtOH | N/A | 0.7893 | 1.201 | 22.8 | 1.3605 | 5.852 | |
| EtOH−$H_2O$ | 20 vol % | 0.9687 | 2.138 | 38.4 | 1.3469 | N/A | |
| | 40 vol % | 0.9352 | 2.840 | 29.9 | 1.3583 | N/A | |
| | 60 vol % | 0.8911 | 2.542 | 27.0 | 1.3638 | N/A | |
| | 80 vol % | 0.8436 | 1.877 | 24.8 | 1.3658 | N/A | |
| zirconyl nitrate dihydrate aqueous solutions | 10 | 0.9821 | 1.120 | 71.8 | 1.3330 | N/A | measured/calculated data in our laboratory |
| | 50 | 0.9866 | 1.250 | 71.7 | 1.3334 | N/A | |
| | 1.0 × $10^2$ | 0.9916 | 1.380 | 71.0 | 1.3345 | N/A | |
| | 5.0 × $10^2$ | 1.076 | 1.500 | 69.8 | 1.3352 | N/A | |
| | 1.0 × $10^3$ | 1.166 | 1.970 | 66.8 | 1.3520 | N/A | |

[a] Except water. [b] Refractive indices of solutions/suspensions were calculated by the Maxwell Garnett mixing rule. [c] Reference 32.

$2H_2O$) aqueous solutions with different concentrations were selected as precursors. All chemicals were purchased from Kanto Chemical, Tokyo, Japan, and used without further treatment. A temperature profile, ranging from 473, 573, 673, 773, to 873 K, was selected for producing particles. Nitrogen was chosen as the carrier gas and was varied from 1.67 × $10^{-5}$ to 1.33 × $10^{-4}$ m$^3$/s. Based on our computer fluid dynamic calculation, the regime in the reactor can be assumed to be a plug flow, and the corresponding residence time of gas inside the reactor can also be calculated (i.e., in several seconds) depending on operational conditions. For comparison, the atomizers and the other spray parts used in the spray pyrolysis experiments were the same as those used in the droplet size measurements.

**2.5. Characterization of Spray Pyrolyzed Particles.** Morphology, mean size, and size distribution of the captured particles from spray pyrolysis experiments were examined by field emission scanning electron microscopy (FE-SEM, S-5000, Hitachi Ltd., Tokyo, Japan) operated at 20 kV. The geometric mean diameter (Feret diameter, $d_p$) and geometric standard deviation (GSD, $\sigma$) were determined by randomly sampling more than 200 particles from FE-SEM photographs. Assuming that all particles are ideal spheroids, the geometric diameter can be transformed into the volume mean diameter, $d_{p,v}$, using the number frequency distribution equation, $d_{p,v} = [\sum(\Delta N d_p^3)/N]^{1/3}$, where $N$ is the number of particles.[4]

## 3. Results and Discussion

**3.1. Droplet Size Measurement.** Pure water was first used as a model precursor for investigation. Effects of water temperature ($T$), spray volume rate ($Q_w$ and $Q_l$), carrier gas flow rate ($Q_g$), and addition of ethanol were analyzed. For $ZrO(NO_3)_2$ aqueous solutions, the effect of precursor concentration was investigated.

**3.1.1. Effect of Water Temperature.** The droplet size distribution of pure water at different temperatures is shown in Figure 2a. The spray power level, $V$, and carrier gas flow rate were kept constant at 5 (50% of the maximum power level) and 3.33 × $10^{-5}$ m$^3$/s, respectively. It is clear that the droplet size distribution changed with temperature variation. For example, only one main peak was found at 6.02 $\mu$m at low temperature (e.g., 288 K). The main peak began to split into two peaks as temperature increased. Bimodal peaks were clearly indicated when temperature increased to 313 K. The phenomena obtained were directly related to the increased spray volume rate with increasing temperatures, as seen in the inset in Figure 2a. For example, in the case of 288 K, the spray volume rate was only about 2.78 × $10^{-9}$ m$^3$/s; however, it increased to about 6.95 × $10^{-9}$ m$^3$/s at 313 K. Meanwhile, the mean droplet size decreased from 6.02 to 4.96 $\mu$m, accordingly. The droplet number concentration was then calculated from 7.30 × $10^{11}$ droplets/m$^3$ (288 K) to 3.26 × $10^{12}$ droplets/m$^3$ (313 K), based

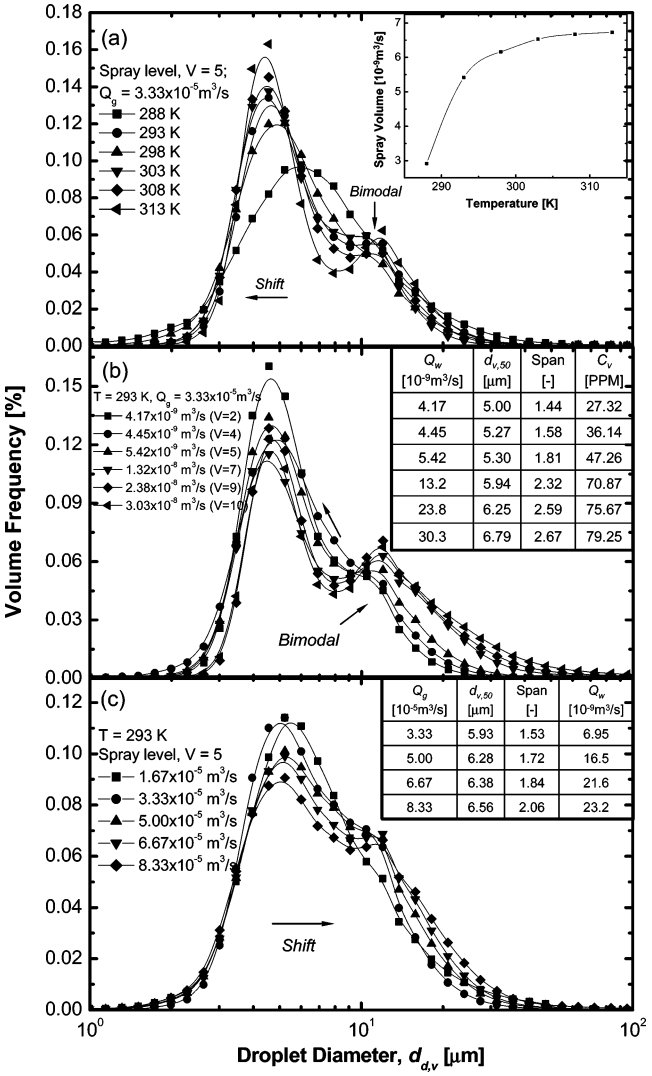


| $Q_w$ [$10^{-9}$ m$^3$/s] | $d_{v,50}$ [μm] | Span [-] | $C_v$ [PPM] |
|---|---|---|---|
| 4.17 | 5.00 | 1.44 | 27.32 |
| 4.45 | 5.27 | 1.58 | 36.14 |
| 5.42 | 5.30 | 1.81 | 47.26 |
| 13.2 | 5.94 | 2.32 | 70.87 |
| 23.8 | 6.25 | 2.59 | 75.67 |
| 30.3 | 6.79 | 2.67 | 79.25 |

| $Q_g$ [$10^{-5}$m$^3$/s] | $d_{v,50}$ [μm] | Span [-] | $Q_w$ [$10^{-9}$m$^3$/s] |
|---|---|---|---|
| 3.33 | 5.93 | 1.53 | 6.95 |
| 5.00 | 6.28 | 1.72 | 16.5 |
| 6.67 | 6.38 | 1.84 | 21.6 |
| 8.33 | 6.56 | 2.06 | 23.2 |

**Figure 2.** Droplet size distribution of pure water at different (a) temperatures, (b) spray power levels, and (c) carrier gas flow rates.

on the equation

$$C_{n,w} = \frac{Q_w}{V_d Q_g} = \frac{10^8}{\pi} \frac{Q_w}{d_{v,50}{}^3 Q_g} \quad (4)$$

Due to the relatively high droplet number concentration, coagulation between droplets occurred and formed bimodal peaks at 313 K. This is in agreement with previous results reported by Messing et al.; that is, the droplet coagulation is relatively insensitive to ambient temperature but strongly dependent on the initial number concentration of droplets.[22] Under conditions similar to this experiment, laminar and turbulent coagulation of droplets may occur, in which the coagulation rate is proportional to the third order of droplet diameter ($d_d{}^3$). In particular, turbulent coagulation plays an important role in the coagulation of aerosol particles larger than a few micrometers even under the small value of $\epsilon_0$, as discussed in previous papers by Okuyama et al.[23,24] The effect of spray volume rate will be explained in detail in the next section. The increased spray volume rate of water at elevated temperatures was due to the decrease of water viscosity and surface tension (Table 1). In addition, from eq 2, the mean droplet size is directly proportional to viscosity and surface tension. The decreased viscosity and surface tension lead to a decrease in mean droplet size, which explains the results from the present experiment. The slightly decreased density had no significant influence on mean droplet size. Further, surface evaporation of water droplets during the increasing temperatures may also have had some influence on mean droplet size. Table 1 shows that the vapor pressure of water at 313 K is about 4.3 times the value at 288 K, indicating a higher evaporation rate at higher temperatures. To investigate other effects, the precursor temperature was kept constant at 293 K in all subsequent measurements.

**Table 2. Droplet Number Concentrations of Pure Water and 1.0 × $10^2$ mol/m$^3$ $ZrO(NO_3)_2$ Aqueous Solution at 293 K, $Q_g$ = 3.33 × $10^{-5}$ m$^3$/s, and Different Spray Power Levels**

| $V$ | $Q_w$ [m$^3$/s] | $C_{n,w}$ [droplets/m$^3$] | $Q_l$[a] [m$^3$/s] | $C_{n,l}$ [droplets/m$^3$] |
|---|---|---|---|---|
| 2 | $4.17 \times 10^{-9}$ | $1.91 \times 10^{12}$ | $3.34 \times 10^{-9}$ | $2.08 \times 10^{12}$ |
| 4 | $4.45 \times 10^{-9}$ | $2.04 \times 10^{12}$ | $3.48 \times 10^{-9}$ | $2.17 \times 10^{12}$ |
| 5 | $5.42 \times 10^{-9}$ | $2.48 \times 10^{12}$ | $4.59 \times 10^{-9}$ | $2.36 \times 10^{12}$ |
| 7 | $1.32 \times 10^{-8}$ | $6.05 \times 10^{12}$ | $6.67 \times 10^{-9}$ | $4.16 \times 10^{12}$ |
| 8 | $1.72 \times 10^{-8}$ | $7.89 \times 10^{12}$ | $9.87 \times 10^{-9}$ | $6.16 \times 10^{12}$ |
| 9 | $2.38 \times 10^{-8}$ | $1.09 \times 10^{13}$ | $1.58 \times 10^{-8}$ | $9.89 \times 10^{12}$ |
| 10 | $3.03 \times 10^{-8}$ | $1.39 \times 10^{13}$ | $2.08 \times 10^{-8}$ | $1.30 \times 10^{13}$ |

[a] For 1.0 × $10^2$ mol/m$^3$ $ZrO(NO_3)_2$ aqueous solution.

**3.1.2. Effect of Spray Volume Rate.** Spray volume rate is another important factor. Changing the spray power level of the ultrasonic nebulizer can control the spray volume rate of precursors. The spray volume rates of pure water, $Q_w$, and $ZrO(NO_3)_2$ aqueous solutions, $Q_l$, increased with increasing spray power levels (Table 2).

Droplet size distributions of pure water at different spray power levels were plotted in Figure 2b. Only one main peak, at around 5.0 $\mu$m, was found in the case of low spray power levels, such as at $V = 2$ ($4.17 \times 10^{-9}$ m$^3$/s). However, bimodal distribution was apparently observed in the cases of higher spray power levels, in which the intensity of the second peak at around 10.0 $\mu$m was found to increase with increasing spray power levels. Meanwhile, the peak intensity of the first peak decreased gradually. The volumetric mean diameter, $d_{v,50}$, and the span of the droplet size distribution were also found to have the same tendency as the second peak intensity (see the inset in Figure 2b), indicating that the size distribution of droplets at high spray volume rates was broad. The same phenomena were observed for 1.0 × $10^2$ mol/m$^3$ $ZrO(NO_3)_2$ aqueous solution (see Supporting Information, Table S1). Interestingly, the bimodal size distribution of both precursors started from the same spray power level, i.e., $V = 7$. In Table 2, the calculated droplet number concentration ($C_n$) increased with increasing spray volume rate. For instance, the droplet number concentration of pure water at a spray volume rate of $4.17 \times 10^{-9}$ m$^3$/s ($V = 2$) was $1.91 \times 10^{12}$ droplets/m$^3$; however, the value increased to $1.39 \times 10^{13}$ droplets/m$^3$ at a spray volume rate of $3.03 \times 10^{-8}$ m$^3$/s ($V = 10$). The high droplet number concentration and large droplet size (i.e., in micrometer size range) are considered the main reasons for the laminar and turbulent coagulation of droplets, as explained above. These results indicate that the coagulation will occur if the droplet number concentration is higher than $3.0 \times 10^{12}$ droplets/m$^3$.

To explain the phenomena (i.e., bimodal size distribution of droplets) more specifically, basic mechanisms of ultrasonic atomization should be introduced as well. Generally, there are two major hypotheses, i.e., capillary wave hypothesis and cavitation hypothesis, that explain the mechanism of liquid disintegration during ultrasonic atomization.[16,25] Bouguslavskii and Eknadiosyants coupled these two hypotheses and proposed a "conjunction theory",[26] according to which the periodic hydraulic shock from the cavitation disturbance interacts with the finite amplitude capillary waves and excites them to form

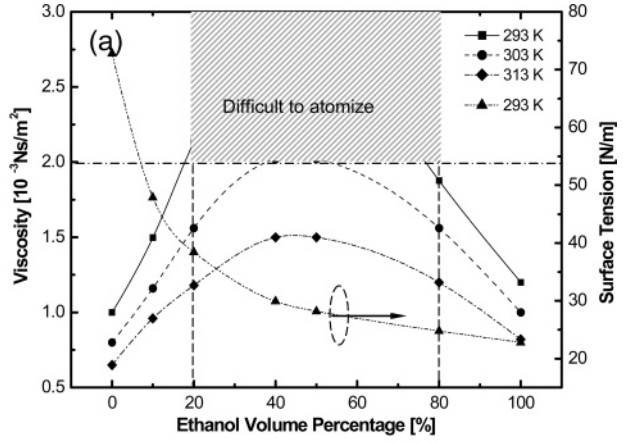


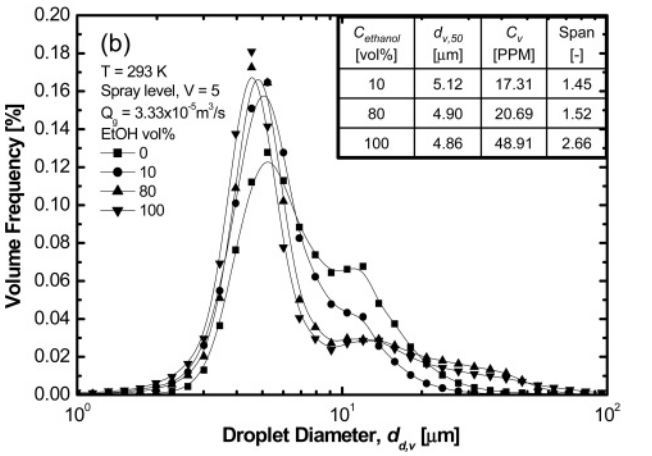


**Figure 3.** (a) Physicochemical properties and (b) droplet size distribution of water−alcohol solutions.

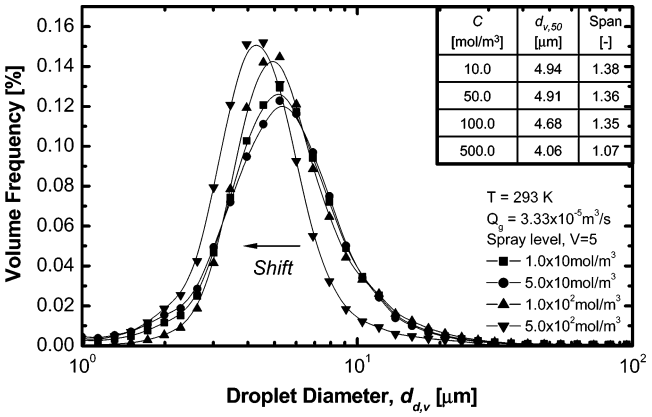


**Figure 4.** Droplet size distribution of $ZrO(NO_3)_2$ aqueous solutions with different concentrations.

droplets. The capillary waves modulated by ultrasonic vibration are regular in nature, which is the reason for uniform droplet distribution. However, the cavitation shock often leads to an irregular random disintegration, which will lead to the broadening of droplet size distribution rather than the production of droplets having a bimodal distribution.[27] On the other hand, the droplet coagulation is accelerated by increasing the initial droplet number concentration.[22] The dramatic increase in the droplet number concentration (spray volume rate), due to the increase of atomization power, precursor temperature, and carrier gas flow rates (which will be discussed in the following section), strongly supports that the bimodal size distribution of droplets in this work is caused by the coagulation.

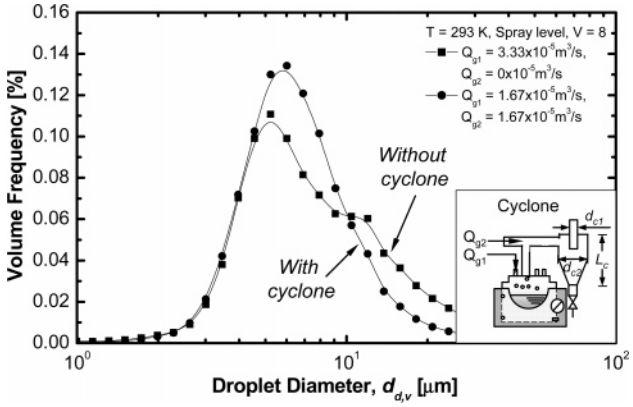


**Figure 5.** Droplet size distribution of pure water using a cyclone.

**3.1.3. Effect of Carrier Gas Flow Rate.** Beside the parameters investigated above, the carrier gas flow rate is also considered to play an important role in droplet size measurement. Droplet size distribution at the spray power level of 5 with different carrier gas flow rates was plotted in Figure 2c. The droplet size distribution became broader when the carrier gas flow rate was increased. For instance, the span at $3.33 \times 10^{-5}$ m$^3$/s was 1.53; the value increased to 2.06 at $8.33 \times 10^{-5}$ m$^3$/s, implying that polydispersed droplets were formed (Figure 2c). Further, the second peak in the size distribution was found when carrier gas flow rate increased to $5.0 \times 10^{-5}$ m$^3$/s. Meanwhile, the mean droplet diameter increased with increasing carrier gas flow rate. In addition, as shown in the inset in Figure 2c, the spray volume of pure water ($Q_w$) was also found to increase with increasing carrier gas flow rate, which agreed well with previous results reported by Rajan et al.[16] These results can be explained by two factors. Large and small droplets were carried out together in the case of high carrier gas flow rates, which was the main reason for the broad droplet size distribution. Laminar and turbulent coagulation of droplets occurred due to increased spray volume rate, and turbulence with increased gas flow rate may be the second reason for the phenomena (see inset in Figure 2c). Similar results were also obtained for $1.0 \times 10^2$ mol/m$^3$ $ZrO(NO_3)_2$ aqueous solution (see Supporting Information, Figure S1).

**3.1.4. Effect of Ethanol Addition.** In spray pyrolysis, aqueous solutions of inorganic salts are frequently used as precursors, due to their safety, availability, easy handling, and high solubility. However, addition of organic compounds, such as alcohol, is sometimes necessary to change the physicochemical properties of the precursor for reduction reaction or combustion.[28,29] In this work, the effect of the addition of ethanol to pure water was analyzed. Four volume concentrations of ethanol−water solutions were chosen, i.e., 10, 20, 80, and 100 vol %. From Figure 3a, it is apparent that the viscosity of the ethanol−water solution had a little complex distribution. The viscosity at 10 vol % ethanol addition at 293 K was only about $1.50 \times 10^{-3}$ N s/m$^2$. The viscosity then increased dramatically with increasing ethanol volume percentages, and reached a maximum value of $2.84 \times 10^{-3}$ N s/m$^2$ at around 40 vol %. After that, a decrease was observed, and the value at 80 vol % ethanol addition was only about $1.80 \times 10^{-3}$ N s/m$^2$. In contrast with viscosity, the surface tension of ethanol−water solution showed a simple decreasing curve with increasing volume percentage of ethanol, due to the decreased intermolecular forces.[30]

In Figure 3b, it was found that the mean droplet diameter decreased with increasing ethanol volume percentages. This may be due to the dramatic decrease of surface tension of the

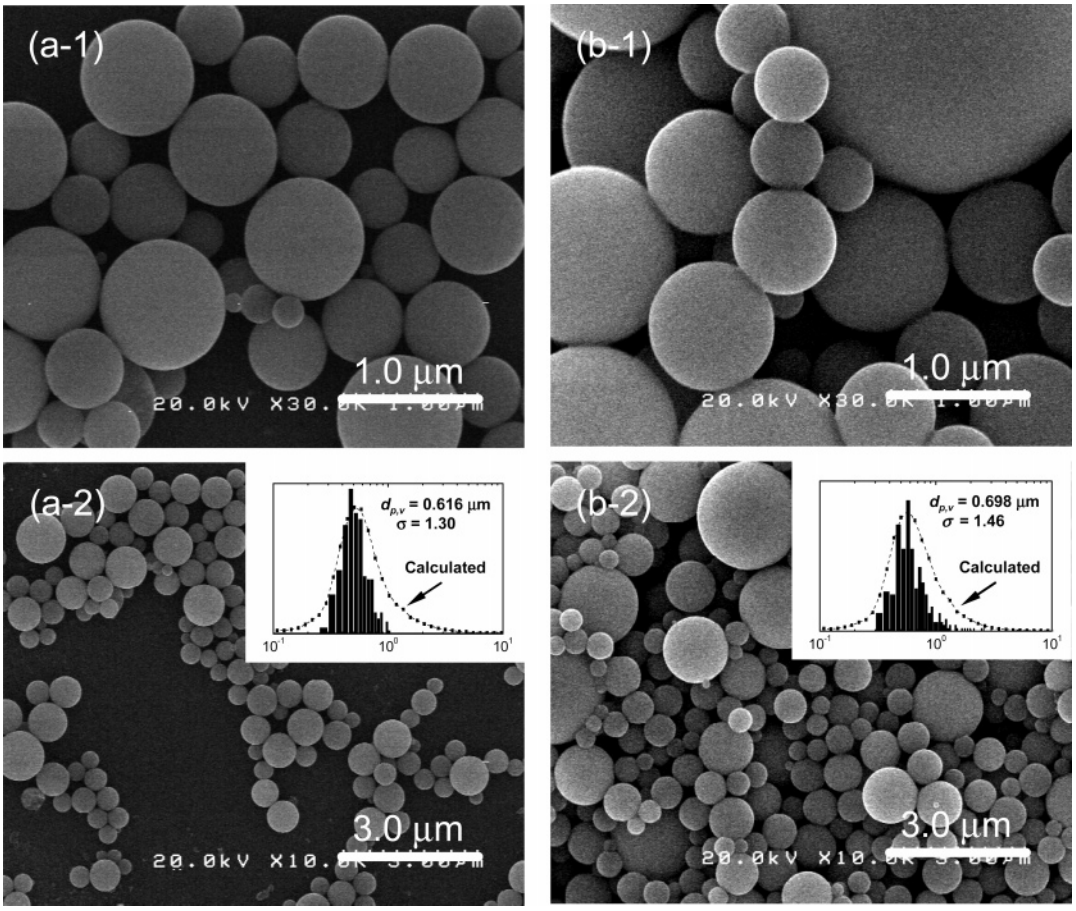


**Figure 6.** FE-SEM images of $ZrO_2$ particles prepared at the spray power level $V = 5$, and different carrier gas flow rates of (a-1, a-2) $1.67 \times 10^{-5}$ $m^3/s$ and (b-1, b-2) $5.00 \times 10^{-5}$ $m^3/s$.

**Table 3. Particle Size Data Measured from FE-SEM Images**

| | conditions | $d_{v,50}$ [$\mu$m] | $d_{p,cal}$ [$\mu$m] | $d_{p,v}$ [$\mu$m] | $\sigma$ |
|---|---|---|---|---|---|
| effect of carrier gas flow rate ($ZrO_2$) | $1.67 \times 10^{-5}$ $m^3/s$ | 4.64 | 0.605 | 0.616 | 1.30 |
| | $3.33 \times 10^{-5}$ $m^3/s$ | 4.84 | 0.631 | 0.625 | 1.36 |
| | $5.00 \times 10^{-5}$ $m^3/s$ | 5.16 | 0.672 | 0.698 | 1.46 |
| | $6.67 \times 10^{-5}$ $m^3/s$ | 5.58 | 0.727 | 0.792 | 1.50 |
| effect of cyclone ($ZrO_2$) | without cyclone, $V = 2$ | 4.51 | 0.588 | 0.578 | 1.28 |
| | without cyclone, $V = 10$ | 5.44 | 0.779 | 0.873 | 1.68 |
| | with cyclone $V = 2$ | 4.27 | 0.556 | 0.544 | 1.25 |
| | with cyclone, $V = 10$ | 4.74 | 0.618 | 0.599 | 1.34 |
| effect of spray power level (NiO) | $V = 2$ | 4.18 | 0.742 | 1.20 | 1.26 |
| | $V = 10$ | 4.72 | 0.838 | 1.27 | 1.61 |

ethanol−water solution, based on eq 2. The viscosity, however, did have some influences on atomization, instead of mean droplet size. As shown in Figure 3b, the droplet volume concentration, $C_v$, increased with the increasing ethanol addition volume. However, it was also observed that the precursors with the ethanol volume percentages from 20% to 80% could not be atomized, due to their very high viscosity (larger than $2.0 \times 10^{-3}$ N s/$m^2$), despite their relatively low surface tension. These results suggested that the viscosity of $2.0 \times 10^{-3}$ N s/$m^2$ may be a critical value for atomization in our current ultrasonic nebulizer. Precursors with viscosity lower than $2.0 \times 10^{-3}$ N s/$m^2$ can be atomized; above that level, no droplets will be formed. Increasing precursor temperature is a possible solution for this problem. From Figure 3a, it can be seen that the viscosity of ethanol−water solution decreased with increasing temperature. However, increasing the precursor temperature increased the spray volume rate and the droplet number concentration. Bimodal droplets may be obtained as described above.

**3.1.5. Effect of Solution Concentration.** To increase the productivity of the particles, it is always preferable to use precursors with high concentrations in the spray pyrolysis process. In prediction of mean particle size based on the ODOP principle, the corresponding mean droplet sizes of precursors with different concentrations have usually been considered to be constant.[4] In fact, droplet characteristics (e.g., size distribution) will change due to variation of physicochemical properties of precursors. The effect of concentration change for a $ZrO(NO_3)_2$ aqueous solution was investigated. Four concentrations of the precursor were selected: 10.0, 50.0, $1.0 \times 10^2$ , and $5.0 \times 10^2$ mol/$m^3$. Figure 4 shows the droplet size distribution of $ZrO(NO_3)_2$ solutions at different concentrations. The results show that the volumetric mean droplet diameter decreased as concentration increased. For example, a mean droplet size of 4.94 $\mu$m at 10.0 mol/$m^3$ decreased to 4.06 $\mu$m at $5.0 \times 10^2$ mol/$m^3$. Meanwhile, the span of the droplet size distribution showed a tendency similar to that of mean droplet size, indicating that droplets with higher unimodal distribution could be obtained at higher concentrations. In addition, only a single peak was found for each concentration in Figure 4, indicating that no droplet coagulation occurred. Detailed droplet size

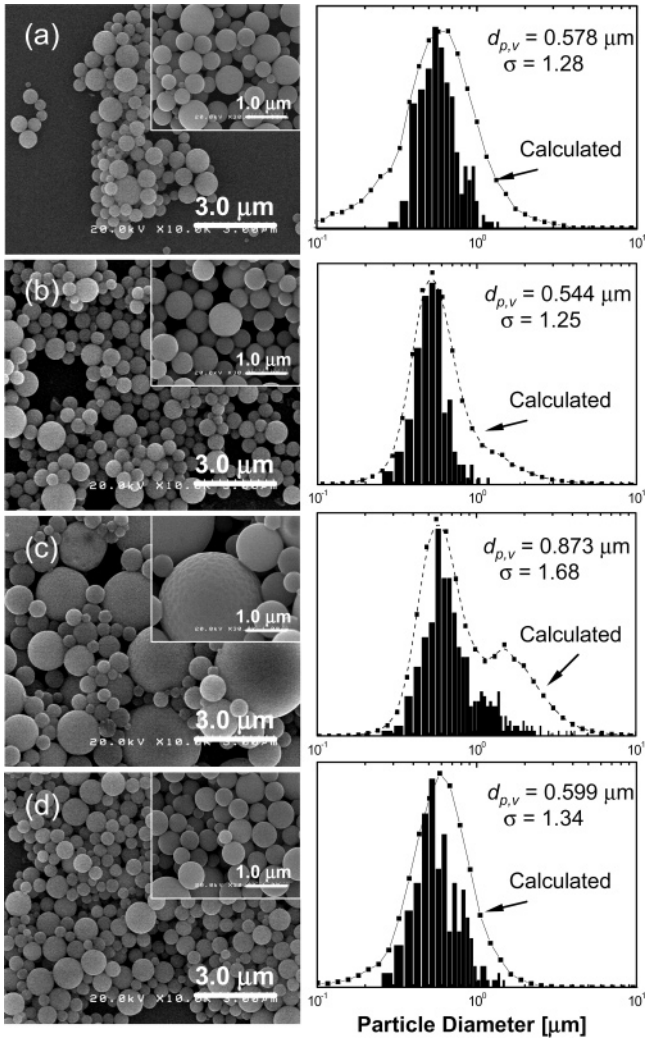


**Figure 7.** FE-SEM images and particle size analysis of $ZrO_2$ prepared at different conditions: (a) $V = 2$, without cyclone; (b) $V = 2$, with cyclone; (c) $V = 10$, without cyclone; and (d) $V = 10$, with cyclone.

measurement data can be found in the Supporting Information (Table S1).The results can be explained by the variation of their physicochemical properties. Table 1 shows that the viscosity and density of $ZrO(NO_3)_2$ aqueous solutions increased with increasing concentration, while the surface tension of the solutions showed a slight decrease. This may be attributed to the decrease in mean droplet size. The viscosity had no significant influence on droplet size variation, as explained above, which mainly controlled the atomization capability of the ultrasonic nebulizer. In other words, for making a liquid jet (then a droplet, from the instable jet), it is necessary to exceed a critical value of the minimum viscosity of a spraying liquid. For instance, droplets did not form when precursors with concentrations higher than $5.0 \times 10^2$ mol/m$^3$ were used, since the viscosity was very high. The viscosity was $1.97 \times 10^{-3}$ N s/m$^2$ at $1.0 \times 10^3$ mol/m$^3$, which is close to the proposed critical viscosity of $2.0 \times 10^{-3}$ N s/m$^2$. Further, the droplet number concentrations of $ZrO(NO_3)_2$ solutions at different concentrations were calculated. The $C_{n,l}$ at each concentration was lower than that of pure water. For example, $2.54 \times 10^{12}$, $2.45 \times 10^{12}$, $2.36 \times 10^{12}$, and $2.0 \times 10^{12}$ droplets/m$^3$ were obtained at 10.0, 50.0, $1.0 \times 10^2$, and $5.0 \times 10^2$ mol/m$^3$, respectively, which were below our proposed critical data for droplet coagulation as shown in section 3.1.2, i.e., $3.0 \times 10^{12}$ droplets/m$^3$. The results show that the concentration of precursor had some effect on mean droplet size and on atomization, both of which predict the particle size based on the ODOP principle.

**3.2. Control of Droplet Size Distribution.** As shown above, the droplet size distribution varied depending on the precursor properties and operation conditions. Bimodal peaks were frequently observed due to laminar and turbulent coagulation of droplets, especially in the cases of high spray volume rates and carrier gas flow rates. To get uniform particles, droplet size distribution should be controlled. Many devices can be used for this purpose, such as impactors, metal meshes, and cyclones. In this work, a cyclone connector and a T-type impactor were used to remove large droplets.

A homemade cyclone connector is schematically shown in Figure 5, where the diameters of inlet and outlet ($d_{c1}$) are $2.0 \times 10^{-2}$ m and the diameter ($d_{c2}$) and the length of the cyclone body ($L_c$) are $5.0 \times 10^{-2}$ m and $1.05 \times 10^{-1}$ m, respectively. The carrier gas flowed two ways through this cyclone connector. The first line ($Q_{g1}$) was connected to the ultrasonic nebulizer to carry atomized droplets out; the second line ($Q_{g2}$) put droplets directly forward horizontally from the cyclone. The second line removed large droplets. The measurements of pure water were carried out at the total carrier gas flow rate of $3.33 \times 10^{-5}$ m$^3$/s with a spray power level of 8 (i.e., 80% of the maximum power of the nebulizer). In Figure 5, a bimodal size distribution was obtained without using a cyclone. A sharp size distribution was achieved after using the cyclone to remove large droplets, as the mean droplet diameter decreased from 6.48 to 5.97 $\mu$m. Similar results were achieved for a $1.0 \times 10^2$ mol/m$^3$ $ZrO(NO_3)_2$ aqueous solution (see Supporting Information, Figure S2). The results indicate that the cyclone is a useful tool for controlling droplet size distribution. The size distribution comparison between spray pyrolyzed particles using the cyclone will be investigated in the following section. Besides, a T-type impactor was also used to control droplet mean size and size distribution. Figure S3 shows how the droplet curve shape became sharp when a T-type impactor was used. Detailed droplet size data can be found in Table S1.

**3.3. Correlations between Particle/Droplet Sizes.** To investigate the relationship between droplets and their corresponding spray pyrolyzed particle sizes, a few experiments synthesizing particles were carried out. For comparison, the same ultrasonic nebulizer was used.

As previously explained, the ODOP principle is considered to be the typical particle formation mechanism in conventional spray pyrolysis (CSP). Assuming that the spray pyrolyzed particles are dense with spherical morphology, based on the mass conservation law, the relationship between the mean droplet size and the corresponding mean particle size is shown as follows:[4]

$$d_{p,v} = d_{d,v}\left(\frac{MC}{\rho_p}\right)^{1/3} \quad (5)$$

In spray pyrolysis, the product particles, e.g., metal oxides, are formed from thermal reactions of precursors. For example, $ZrO(NO_3)_2$ will undergo decomposition to form $ZrO_2$ under high temperatures.

Figure 6 shows FE-SEM images of $ZrO_2$ particles prepared at the spray power level of 5, with different carrier gas flow rates of $1.67 \times 10^{-5}$ m$^3$/s (Figure 6a) and $5.0 \times 10^{-5}$ m$^3$/s (Figure 6b). From the FE-SEM images, the particles prepared were all perfectly spherical in morphology. The measured volumetric mean diameters of the resulting particles were in good agreement with those calculated from the corresponding mean droplet sizes. For example, in the case of low carrier gas flow rate, i.e., $1.67 \times 10^{-5}$ m$^3$/s, the measured particle size

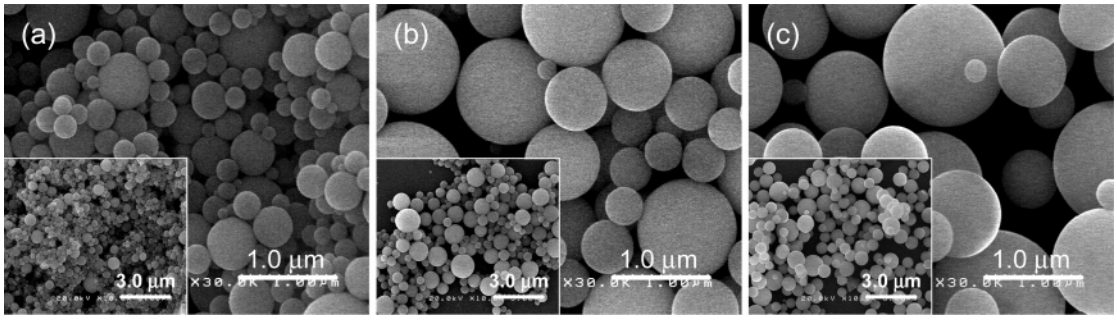


**Figure 8.** FE-SEM images of $ZrO_2$ particles prepared at different concentrations: (a) 10.0, and (b) 50.0, and (c) $5.0 \times 10^2$ mol/m$^3$.

was 0.616 $\mu$m with a GSD of 1.30. The calculated mean particle size was 0.605 $\mu$m from the corresponding mean droplet size using eq 5. The error between the two diameters was less than 2%, indicating that the resulting particles were solid/dense ones. High carrier gas flow rate resulted in a slightly larger particle size, i.e., 0.698 $\mu$m (Figure 6b) with a bigger GSD (1.46), due to the characteristics of corresponding droplet size distributions (as seen in Table 3). These findings indicate that the resulting particles were almost uniform at the spray power level of 5, since the GSD was smaller than 1.5. However, at a higher spray power level, i.e., $V = 10$, the particle size distribution was predicted to be broader from the corresponding droplet characteristics, in which lager droplets should be removed leaving uniform particles.

Figure 7 shows FE-SEM images of $ZrO_2$ particles prepared without using a cyclone (Figure 7a,c) and with a cyclone (Figure 7b,d) at the different spray power levels. In Figure 7, the particle size distribution was sharp at the low spray power level. The corresponding GSDs of these particles were 1.28 without using the cyclone and 1.25 using the cyclone (Figure 7a,b). There was little difference between the mean size and size distribution of particles prepared under both conditions, implying that at low spray power levels removing large droplets is unnecessary. However, at the high spray power level of $V = 10$, the particle size distribution was very broad. Figure 7c shows how many large particles mixed with fewer small particles. The mean particle diameter measured from FE-SEM images was 0.873 $\mu$m, with a GSD of 1.68. The mean particle size and particle size distribution coincided with those calculated from the corresponding droplet size data. After using the cyclone to remove large droplets, uniform particles with a mean particle size of 0.599 $\mu$m and a smaller GSD of 1.34 were observed (Figure 7d). Figure 7 shows that for all cases, the droplet size distribution (dotted line) calculated from the corresponding droplet size distribution was slightly broader than the measured particle size distribution (vertical column), although the shapes were very similar. This phenomenon may have resulted from the difference between the measurement methods for particle and droplet sizes, since the mean particle diameters were determined by randomly sampling about 200 particles from FE-SEM photographs, while the calculated particle size distribution was based on droplet size distribution, in which all droplets were assumed to be transferred to particles. The results showed that mean size and size distribution of particles prepared by the spray pyrolysis method had a strong relationship with the physical properties of spraying droplets. Uniform particles can be obtained by controlling the droplet size distribution, using either a cyclone connector or a T-type impactor.

To investigate the concentration effect, $ZrO_2$ particles from $ZrO(NO_3)_2$ aqueous solutions with different concentrations were synthesized. Figure 8 shows that spherical particles were obtained in all cases. The mean droplet sizes were 4.94, 4.91,

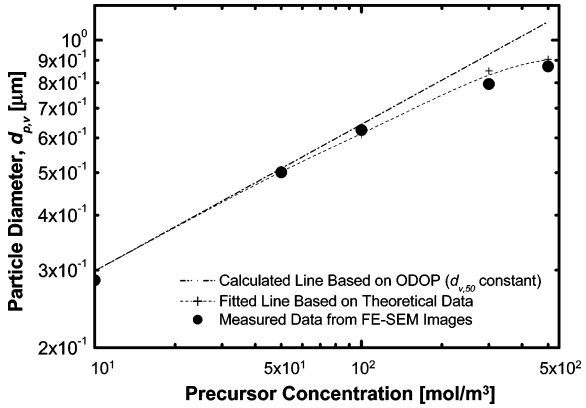


**Figure 9.** Comparison of mean diameters of $ZrO_2$ particles between theoretical values and measured data from corresponding FE-SEM images.

and 4.06 $\mu$m at 10.0, 50.0, and $5.0 \times 10^2$ mol/m$^3$, respectively (also refer to Figure 4). The corresponding calculated particle sizes based on the ODOP principle were 0.299, 0.508, and 0.905 $\mu$m, respectively, which are indicated as theoretical data in Figure 9. The measured mean diameters from their corresponding FE-SEM images were 0.285, 0.501, and 0.871 $\mu$m, respectively. The average errors between the calculated and measured data were less than 1.0%, indicating the good agreement (fitted line in Figure 9).

On the other hand, as reported previously, the mean droplet sizes were always assumed to be constant at different concentrations.[4] The particle mean size showed a linear relationship with the precursor concentration following eq 5 with its logarithmic form:

$$\log(d_{p,v}) = \frac{1}{3}\log C + \log\left(d_{d,v}\left[\frac{M}{\rho_p}\right]^{1/3}\right) \qquad (6)$$

where the slope is 1/3, and the intercept is $\log(d_{d,v}[M/\rho_p]^{1/3})$.[4] With the assumption that the mean droplet diameter was constant at 4.94 $\mu$m, which was the measured data at 10.0 mol/m$^3$, the calculated line of the particle mean diameter versus the precursor concentration based on eq 6 is shown in Figure 9. This agreed with the measured data in low concentrations; however, large errors occurred at high concentrations. This means that particle size cannot be predicted precisely using an assumed constant mean droplet size for a wide range of concentrations. In real cases, calculated particle sizes based on real measured droplet sizes at different concentrations should be used for comparison, since the droplet size characteristics change with the variation of precursor concentration, as discussed above.

It should be noted that particle formation during spray pyrolysis is actually a complex process, which involves many physical and chemical phenomena, such as evaporation, nucleation, crystal growth, drying, thermal reactions, and sintering.

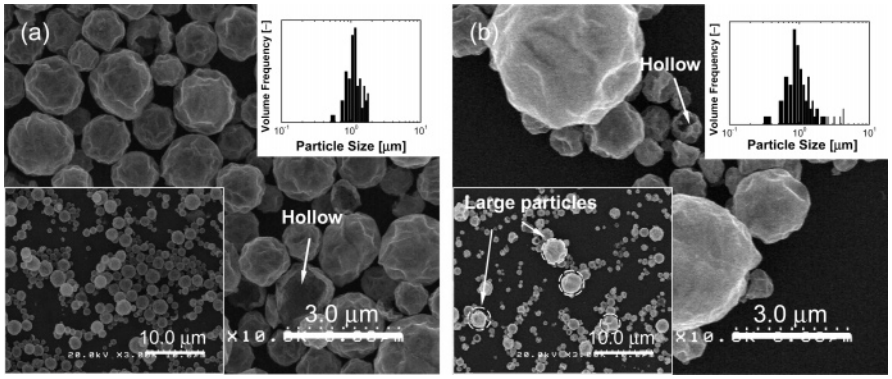


**Figure 10.** FE-SEM images of NiO particles prepared at different spray power levels: (a) $V = 2$ and (b) $V = 10$.

Besides droplet mean size and size distribution, particle mean size, size distribution, and morphology are also dependent on the physicochemical properties of precursors, the operational conditions, and the thermal reactions.

For comparison, $1.0 \times 10^2$ mol/m$^3$ nickel nitrate aqueous solution was also ultrasonically sprayed to produce nickel oxide particles at two spray power levels: $V = 2$ and $V = 10$. Figure 10 shows that the spray pyrolyzed particles had hollow morphology with wrinkled surfaces. The measured particle sizes from the FE-SEM images were larger than those calculated from their corresponding mean droplet sizes. In the case of $V = 2$ (Table 3), the measured particle size from the FE-SEM image was 1.20 $\mu$m, which was much larger than the calculated particle size (0.742 $\mu$m). Hollow particle formation is frequently found in the spray pyrolysis process, depending on the physicochemical properties of precursors, carrier gas flow rate, operating temperatures, inner diameter/length of reactor, and other factors. Since the formation of hollow particles involves complex phenomena during the spray pyrolysis process, it is difficult to directly predict particle sizes from their corresponding mean droplet sizes. However, from FE-SEM images in Figure 10, it is clear that the particle size distribution was sharp at the low spray power level of $V = 2$ (Figure 10a), while a broad particle size distribution was observed at the high spray volume rate of $V = 10$ (Figure 10b). This suggests that, in the case of hollow particle formation, the particle size distribution, rather than particle size, can be predicted from the corresponding droplet size distribution.[3]

## 4. Conclusions

Droplet mean size and size distribution of pure water, $ZrO(NO_3)_2$, and nickel nitrate aqueous/alcohol solutions in ultrasonic spray pyrolysis were analyzed systematically by means of a laser diffraction technique. Effects of precursor temperature, spray volume rate, carrier gas flow rate, addition of ethanol, and precursor concentration were analyzed in detail. These results showed that the mean droplet size decreased with increasing precursor temperature, precursor concentration, and addition of ethanol; however, mean droplet size increased with increasing spray volume rate and carrier gas flow rate. Bimodal droplet size distribution was observed with increasing spray volume rate and carrier gas flow rate, due to laminar and turbulent coagulation of droplets. Viscosity of $2.0 \times 10^{-3}$ N s/m$^2$ and droplet number concentration of $3.0 \times 10^{12}$ droplets/m$^3$ were found to be critical values for atomization and coagulation, respectively. A cyclone connector and a T-type impactor were used to control the droplet mean size and size distribution. Uniform droplets could be obtained using a cyclone under various conditions due to the removal of lager droplets. For comparison, spray pyrolysis of $ZrO(NO_3)_2$ and $Ni(NO_3)_2$ solutions was also conducted. Mean particle size and particle size distribution of the spray pyrolyzed powders were analyzed using scanning electron microscopy (SEM). The results showed that the mean particle size and size distribution were strongly dependent on and could be controlled by the droplet size characteristics.

## Acknowledgment

The authors thank Shunsuke Kinouchi for his assistance in experiments. Japan Society for the Promotion of Science (JSPS) and the Ministry of Education, Culture, Sports, Science and Technology (MEXT) of Japan are acknowledged for providing a postdoctoral fellowship (W.-N.W.), a doctoral scholarship (A.P.), Grants-in-Aid for Scientific Research (K.O., I.W. L.), and Special Coordination Funds for Promoting Science and Technology (I.W.L.).

**Supporting Information Available:** Figure S1, droplet size distribution of $1.0 \times 10^2$ mol/m$^3$ $ZrO(NO_3)_2$ aqueous solution at the spray power level of 5, and different carrier gas flow rates; Figure S2, droplet size distribution of $1.0 \times 10^2$ mol/m$^3$ $ZrO(NO_3)_2$ aqueous solution using a cyclone; Figure S3, droplet size distribution of pure water and $1.0 \times 10^2$ mol/m$^3$ $ZrO(NO_3)_2$ aqueous solution using a T-type impactor; and Table S1, droplet size measurement data under various conditions. This material is available free of charge via the Internet at http://pubs.acs.org.

## Nomenclature

$C$ = precursor concentration [mol/m$^3$]
$C_v$ = droplet volume concentration [ppm]
$C_{n,w}$ = droplet number concentration (water) [droplets/m$^3$]
$C_{n,l}$ = droplet number concentration ($ZrO(NO_3)_2$) [droplets/m$^3$]
$d_{c1}$ = diameter of inlet/outlet of cyclone [m]
$d_{c2}$ = diameter of cyclone body [m]
$d_d$ = mean droplet diameter [m]
$d_{d,v}$ = volumetric diameter of droplet [m]
$d_{v,10}$ = volumetric diameter at 10 vol % [m]
$d_{v,50}$ = volumetric diameter at 50 vol % [m]
$d_{v,90}$ = volumetric diameter at 90 vol % [m]
$d_p$ = product particle size (Feret diameter) [m]
$d_{p,v}$ = volumetric particle diameter [m]
$d_{p,cal}$ = calculated particle diameter [m]
$f$ = frequency of ultrasonic transducer [Hz]
$L_1$ = distance between nozzle and detector/lens [m]
$L_2$ = distance between nozzle exit and laser [m]
$L_c$ = length of cyclone body [m]

$M$ = molecular weight of particle [kg/mol]
$n$ = refractive index
$P$ = vapor pressure [Pa]
$Q$ = liquid flow rate [$m^3/s$]
$Q_w$ = spray volume rate of water [$m^3/s$]
$Q_l$ = spray volume rate of liquid [$m^3/s$]
$Q_g$ = total carrier gas flow rate [$m^3/s$]
$Q_{g1}$ = carrier gas flow rate inside nebulizer [$m^3/s$]
$Q_{g2}$ = carrier gas flow rate outside nebulizer [$m^3/s$]
$T$ = temperature of precursor [K]
$V_d$ = droplet volume($=\pi d_{v,50}^3/6$) [$m^3$]
$V$ = spray power level

*Greek Symbols*

$\eta$ = viscosity of liquid/precursor [N $s/m^2$]
$\rho$ = density of precursor [$kg/m^3$]
$\rho_p$ = density of product material [$kg/m^3$]
$\gamma$ = surface tension of precursor [N/m]
$\sigma$ = geometric standard deviation
$\epsilon_0$ = average energy dissipation rate [$m^2/s^3$]

*Subscripts*

cal = calculated
d = droplet
g = carrier gas
l = liquid
n = number
p = particle
v = volume
w = water

## Literature Cited


(1) Okuyama, K.; Lenggoro, I. W. Preparation of Nanoparticles via Spray Route. *Chem. Eng. Sci.* **2003**, *58*, 537.

(2) Elversson, J.; Millqvist-Fureby, A.; Alderborn, G.; Elofsson, U. Droplet and Particle Size Relationship and Shell Thickness of Inhalable Lactose Particles during Spray Drying. *J. Pharm. Sci.* **2003**, *92*, 900.

(3) Widiyastuti, W.; Wang, W. N.; Lenggoro, I. W.; Iskandar, F.; Okuyama, K. Simulation and Experimental Study of Spray Pyrolysis of Polydispersed Droplets. *J. Mater. Res.* **2007**, *22*, 1888.

(4) Wang, W. N.; Widiyastuti, W.; Lenggoro, I. W.; Kim, T. O.; Okuyama, K. Photoluminescence Optimization of Luminescent Nanocomposites Fabricated by Spray Pyrolysis of a Colloid-Solution Precursor. *J. Elctrochem. Soc.* **2007**, *154*, J121.

(5) Suh, W. H.; Suslick, K. S. Magnetic and Porous Nanospheres from Ultrasonic Spray Pyrolysis. *J. Am. Chem. Soc.* **2005**, *127*, 12007.

(6) Taniguchi, I. Physical and Electrochemical Properties of Spherical Nanostructured $LiCr_xMn_{2-x}O_4$ Particles Synthesized by Ultrasonic Spray Pyrolysis. *Ind. Eng. Chem. Res.* **2005**, *44*, 6560.

(7) Capote, F. P.; de Castro, M. D. L. Ultrasound in Analytical Chemistry. *Anal. Bioanal. Chem.* **2007**, *387*, 249.

(8) Laurell, T.; Petersson, F.; Nilsson, A. Chip Integrated Strategies for Acoustic Separation and Manipulation of Cells and Particles. *Chem. Soc. Rev.* **2007**, *36*, 492.

(9) Guo, L. J.; Li, G. J.; Chen, B.; Chen, X. J.; Papailiou, D. D.; Panidis, T. Study on Gas-liquid Two-phase Spraying Characteristics of Nozzles for the Humidification of Smoke. *Exp. Therm. Fluid Sci.* **2002**, *26*, 715.

(10) Zhang, G. J.; Ishii, M. Isokinetic Sampling Probe and Image-Processing System for Droplet Size Measurement in 2-Phase Flow. *Int. J. Heat Mass Transfer* **1995**, *38*, 2019.

(11) Triballier, K.; Dumouchel, C.; Cousin, J. A Technical Study on the Spraytec Performances: Influence of Multiple Light Scattering and Multi-modal Drop-size Distribution Measurements. *Exp. Fluids* **2003**, *35*, 347.

(12) Blaisot, J. B.; Yon, J. Droplet Size and Morphology Characterization for Dense Sprays by Image Processing: Application to the Diesel Spray. *Exp. Fluids* **2005**, *39*, 977.

(13) Ariyapadi, S.; Balachandar, R.; Berruti, F. Spray Characteristics of Two-phase Feed Nozzles. *Can. J. Chem. Eng.* **2003**, *81*, 923.

(14) Viswanathan, S.; Lim, D. S.; Ray, M. B. Measurement of Drop Size and Distribution in an Annular Two-phase, Two-component Flow Occurring in a Venturi Scrubber. *Ind. Eng. Chem. Res.* **2005**, *44*, 7458.

(15) Heine, M. C.; Pratsinis, S. E. Droplet and Particle Dynamics during Flame Spray Synthesis of Nanoparticles. *Ind. Eng. Chem. Res.* **2005**, *44*, 6222.

(16) Rajan, R.; Pandit, A. B. Correlations to Predict Droplet Size in Ultrasonic Atomisation. *Ultrasonics* **2001**, *39*, 235.

(17) Wang, W. N.; Kim, S. G.; Lenggoro, I. W.; Okuyama, K. Polymer Assisted Annealing of Spray-pyrolyzed Powders for Formation of Luminescent Particles with Submicron and Nanometer Sizes. *J. Am. Ceram. Soc.* **2007**, *90*, 425.

(18) Yasuda, K.; Bando, Y.; Yamaguchi, S.; Nakamura, M.; Oda, A.; Kawase, Y. Analysis of Concentration Characteristics in Ultrasonic Atomization by Droplet Diameter Distribution. *Ultrason. Sonochem.* **2005**, *12*, 37.

(19) Maxwell Garnett, J. C. Colors in Metal Gases and in Metallic Films. *Philos. Trans. R. Soc., A* **1904**, *203*, 385.

(20) Chang, H. W.; Okuyama, K. Optical Properties of Dense and Porous Spheroids Consisting of Primary Silica Nanoparticles. *J. Aerosol Sci.* **2002**, *33*, 1701.

(21) Wang, W. N.; Lenggoro, I. W.; Terashi, Y.; Wang, Y. C.; Okuyama, K. Direct Synthesis of Barium Titanate Nanoparticles via a Low Pressure Spray Pyrolysis Method. *J. Mater. Res.* **2005**, *20*, 2873.

(22) Messing, G. L.; Zhang, S. C.; Jayanthi, G. V. Ceramic Powder Synthesis by Spray-Pyrolysis. *J. Am. Ceram. Soc.* **1993**, *76*, 2707.

(23) Okuyama, K.; Higashitani, K. Agglomeration (Coagulation). In *Powder Technology Handbook*, 3rd ed.; Masuda, H. H. K., Yoshida, H., Eds.; Taylor & Francis Group: New York, 2006; p 183.

(24) Okuyama, K.; Kousaka, Y.; Kida, Y.; Yoshida, T. Turbulent Coagulation of Aerosols in a Stirred Tank. *J. Chem. Eng. Jpn.* **1977**, *10*, 142.

(25) Avvaru, B.; Patil, M. N.; Gogate, P. R.; Pandit, A. B. Ultrasonic Atomization: Effect of Liquid Phase Properties. *Ultrasonics* **2006**, *44*, 146.

(26) Bouguslavskii, Y. Y.; Eknadiosyants, O. K. Physical Mechanism of the Acoustic Atomization of a Liquid. *Sov. Phys. Acoust.* **1969**, *15*, 14.

(27) Topp, M. N.; Eisenklam, P. Industrial and Medical Uses of Ultrasonic Atomizers. *Ultrasonics* **1972**, *10*, 127.

(28) Wang, W. N.; Itoh, Y.; Lenggoro, I. W.; Okuyama, K. Nickel and Nickel Oxide Nanoparticles Prepared from Nickel Nitrate Hexahydrate by a Low Pressure Spray Pyrolysis. *Mater. Sci. Eng., B* **2004**, *111*, 69.

(29) Wang, W. N.; Lenggoro, I. W.; Terashi, Y.; Kim, T. O.; Okuyama, K. One-step Synthesis of Titanium Oxide Nanoparticles by Spray Pyrolysis of Organic Precursors. *Mater. Sci. Eng., B* **2005**, *123*, 194.

(30) McMurry, J.; Fay, R. C. *Chemistry*, 3rd ed.; Prentice Hall: Upper Saddle River, NJ, 2001; p 395.

(31) Lide, D. R. *CRC Handbook of Chemistry and Physics*, 84th ed.; CRC Press: New York, 2004.

(32) Schiebener, P.; Straub, J.; Levelt Sengers, J. M. H.; Gallagher, J. S. Refractive Index of Water and Steam as Function of Wavelength, Temperature and Density. *J. Phys. Chem. Ref. Data* **1990**, *19*, 677.


*Received for review* June 15, 2007
*Revised manuscript received* November 9, 2007
*Accepted* November 29, 2007

IE070821D